Effect of lifter shape and operating parameters on the flow of materials in a pilot rotary kiln: Part IV. Improvement of the hydrodynamics-related dimensionless correlations

Kevin Lachin, Aka Doche, Stéphane Vitu, Marie Debacq

Effect of lifter shape and operating parameters on the flow of materials in a pilot rotary kiln: Part IV. Improvement of the hydrodynamics-related dimensionless correlations

K. LACHIN[a], A. DOCHE[a], S. VITU[a,b], M. DEBACQ[a,b]

[a] Université Paris-Saclay, INRAE, AgroParisTech, UMR SayFood, 91120, Palaiseau, France
[b] Conservatoire National des Arts et Métiers, 2 Rue Conté, 75003 Paris, France

Highlights

- The flow of parallelepipedal particles inside a rotary kiln was studied
- Residence Time Distribution (RTD) experiments were performed with this product
- The experimental mean residence time and axial dispersion coefficient were obtained
- The dimensionless hydrodynamic models of Bongo Njeng et al. were tested
- These models were re-identified and simplified for more accuracy and genericity

Abstract

Non-spherical particles are widely processed in industrial-scale rotary kilns. There is nonetheless a lack of simple tools that make it possible to predict their hydrodynamic behavior inside rotary kilns. This article thus focuses on the hydrodynamics of crozets flowing inside a pilot-scale rotary kiln. Thirty-eight experiments were conducted with this product. Experimental Residence Time Distribution curves were successfully obtained with a tracer pulse methodology using painted crozets. Both the experimental mean residence time and the axial dispersion coefficient were obtained by fitting the analytical expression of $E(t)$ for the open-open boundary condition with the experimental $E(t)$ curves. The hydrodynamic behavior observed was qualitatively in agreement with the literature. Our dimensionless models were then re-identified with all of the experimental data and simplified through statistical analysis. This study provides more robust dimensionless hydrodynamic models that can be used to reliably predict the behavior of non-spherical particle flow inside an industrial kiln.

Keywords

Rotary kiln; dimensionless modeling; residence time distribution; non-spherical particles; granular hydrodynamics; food processing

1. Introduction

Rotary kilns are among the most frequently used gas-solid contactors at the industrial scale. These processes are extensively used for applications that require relatively moderate temperatures (drying) or high temperatures (calcination, incineration) since they allow precise control of the process hydrodynamics and heating properties. Moreover, rotary kilns are intrinsically capable of handling various loads in terms of physical properties and size distribution [1]. For these reasons, we commonly find rotary kilns in industries as diverse as the food industry, mineral processing, waste treatment, etc. While rotary kilns were invented at the end of the 19th century, research efforts on these processes are still going strong for three main reasons. The first reason is related to process optimization in terms of energy consumption and pollutant emissions (gases: CO_2, CO, NOx, SOx and fine particles). As environmental issues increase, there is an urgent need to reduce the impact of polluting industries such as cement production, all of which translates into sustained research efforts on rotary kilns. Secondly, applications gradually emerged, especially related to waste treatment [2–5] and biomass/by-product valorization [6–8]. These applications currently focus considerable research efforts aimed at proposing strategies to conduct and scale-up these processes. Ultimately, despite significant successes and achievements, the fine scientific understanding of the physics occurring inside these processes, together with granular hydrodynamics (using mono or polydisperse media), multiphasic heat transfer and chemical reactions is still a challenge at this time [1]. The Discrete Element Method (DEM) is now a frequently used tool since it makes it possible to numerically consider this complexity and study the influence of parameters related to the product or the process geometry over the heat transfer performances [9,10]. When it comes to hydrodynamics alone, efforts are currently underway on both the microscopic comprehension of the particle motion inside rotary drums and kilns (through simulation tools such as DEM [11,12] or analytical treatment [13]), and the macroscopic understanding of the granular load behavior using the well-known Residence Time Distribution (RTD) methodology [14–18]. This knowledge of hydrodynamic behavior is of prime importance in these processes as it directly impacts the uniformity and the intensity of the heat treatment undergone by particles. A shorter mean residence time than expected will directly impact the product quality, whereas a longer mean residence time will overconsume energy.

Previous articles by our research team [19–22] proposed experimental results and correlations for hydrodynamics-related and thermal-related parameters based on a complete dimensional analysis of the process. This paper continues this combination of experimental and modeling efforts by studying the RTD of a parallelepipedal food product (crozets, regional French pasta) in a rotary kiln. The product's shape, combined with its intrinsic properties, make it a perfect candidate to test the robustness and genericity of these hydrodynamics-related correlations (axial dispersion coefficient D and mean residence time $\bar{t}$ prediction). After discussing the limitations of the previous models, we propose improvements based on model re-identification and statistical analysis. These improvements are ultimately aimed at proposing more robust, generic and easy-to-use hydrodynamic correlations.

2. Theory

Axial dispersion modeling, originally introduced by Danckwerts, considers the 1-D convection-diffusion equation (also known as the Fokker-Planck equation) presented in its generalized form in *(1)*.

$\frac{\partial C}{\partial \theta} = \frac{1}{Pe} . \frac{\partial^2 C}{\partial \zeta^2} - \frac{\partial C}{\partial \zeta}$	*(1)*

In this equation, C denotes the concentration of a species in the considered flow normalized by the inlet tracer concentration, ζ denotes the dimensionless position inside the kiln (z divided by the kiln length L), and θ denotes the dimensionless time (t divided by $\bar{t}$, where $\bar{t}$ stands for the mean residence time).

The Peclet number, or *Pe*, is a well-known and commonly used dimensionless number that compares convection and dispersion (for a solid flow) in terms of characteristic time. The higher the *Pe* is, the less the dispersion and, thus, the more uniform and narrow the concentration distribution will be at the outlet of the considered process. The general expression of *Pe* is given in *(2)*.

$Pe = \frac{u.L}{D}$	*(2)*

u denotes here the mean axial velocity. *Pe* is inversely proportional to the axial dispersion coefficient D. This dispersion coefficient encompasses all the transport phenomena that are not convective, such as turbulence or molecular diffusion. While straightforward, this modeling approach has proven to be effective for modeling the macroscopic hydrodynamic behavior of an extensive range of continuous processes, including processes that deal with solids [23]. When it comes to rotary kilns and drums, a vast quantity of studies can also be found in the literature, demonstrating the relevance of the approach [14–18,20,24,25].

For open-open boundary conditions, the analytical solution of *(1)* can easily be found in the literature [26] and is presented in *(3)*.

$E(\mathrm{t}) = \frac{1}{2} . \sqrt{\frac{Pe}{\pi . t . \bar{t}}} . e^{\left(\frac{-Pe.(\bar{t}-t)^2}{4.t.\bar{t}}\right)}$	*(3)*

Fitting the theoretical expression of *E(t)* to experimental curves thus allows us to experimentally determine *Pe* and $\bar{t}$.

3. Materials and methods

3.1 Materials processed

The previous experimental results of Bongo Njeng et al. [19–21] were obtained using three different types of granular materials: sand, broken rice and beech chips. The main properties of these solids are provided in *Table 1*. For this study, crozets (Alpina, France), typical pasta from Savoie, were considered and characterized in terms of dimensions, bulk density (ρ_{bulk})**,** tapped density (ρ_{tapped}) and angle of repose (θ_p). Crozets are of particular relevance as they exhibit highly non-spherical geometry while having different densities and angles of repose from beech chips. These differences thus make it possible to test the robustness of the hydrodynamic models introduced in [21].

The properties of crozets measured for this study are listed in *Table 1* and can also be found in our "Rotary Kilns and Drums" dataverse *(*see *Data Availability)*, while *Figure 1* presents the visual aspects of this product.

Table 1: Physical properties of the solids used for the experiments

Properties	***Sand***	***Broken rice***	***Beech chips***	***Crozets (this study)***
Shape	Sphere	Cylinder	Rectangular parallelepiped	Rectangular parallelepiped
Dimensions (mm)	0.55	3.8*1.9	10*4.5*2.0	5.5*5.7*2.0
$\boldsymbol{\rho_{bulk}}$ **(kg.m^{-3})**	1460	892	260	668
$\boldsymbol{\rho_{tapped}}$ **(kg.m^{-3})**	1543	931	284	765
$\boldsymbol{\theta_p}$ **(°)**	39.0	26.0	42.0	27.9
Kiln	1	1	2	1
Dataset	[27]	[28]	[29]	[30]

Figure 1: Crozets moving inside the experimental rotary kiln

Dimensions were obtained with the image software, ImageJ (ImageJ 1.53, ImageJ, USA). Tapped density ρ_{tapped} was estimated using a tapping volume meter for 10 min. The occupied solid volume after tapping made it possible to determine the tapped density. Bulk density ρ_{bulk} was determined by measuring the solid mass corresponding to a volume of 50 mL inside a measurement cylinder. All these measurements were performed in triplicate. The angle of repose θ_p was calculated by averaging the results obtained by the fixed cone method [31] and by image analysis with ImageJ.

Despite the highly non-spherical character of the particles used, the rolling regime [32] could be observed for a sufficient hold-up. On the other hand, when the hold-up is low (as seen on *Figure 1*), the sliding regime [32] predominates. We can also observe a "mosaic effect" on this figure: when the inlet mass flow rate is low, the crozets slowly entering the rotating tube rearrange themselves into a flat and tidy layer, like a mosaic.

3.2 Rotary kiln

The rotary kiln used for the experiments is extensively presented elsewhere [19]; associated data is also available [33]. The only difference is that feeding is ensured with a vibrating conveyor (TUXEL-VIB, Model LEV3, Belgium) in this study, and the mass flow rate is controlled by adjusting the vibration intensity of the conveyor. The tubular rotary kiln is built with Incoloy alloy 800 and supported by four rollers. The kiln slope can be varied using a hydraulic jack with a manual pump: the maximal slope value reachable is 5°. Rotation is ensured through a chain and sprocket mechanism by a variable speed motor (180 W DC), allowing a rotation speed of between 2 and 12 RPM. After being processed inside the kiln, the solid is collected inside a recovery tank.

Using lifters inside the kiln impacts both the hydrodynamics and the solid retention. In this study, two configurations are considered: without lifters (NL: no lifters) and with four one-section 10-mm heat-resistant steel straight lifters (referred to as SL), evenly distributed at the periphery of a tubular structure. The structure can be easily added or removed from the kiln, and its length is approximately equal to the length of the kiln tube. Extensive details about these lifters can be found in the "Material and methods" sections of previous papers [19,20]. Open dams of defined heights (13.5, 23.5 and 33.5 mm in this work) can also be placed at the outlet to adjust the solid height inside the kiln. It should be noted that these dam heights do not include the thickness of the tube and thus correspond to the exit bed height.

3.3 RTD measurements

Experimental Residence Time Distributions were obtained by introducing a tracer pulse at the inlet of the process and monitoring the outlet concentration of this tracer over time. All the experiments were performed at ambient temperature and atmospheric pressure. For these experiments, we used dyed crozets as a tracer and we ensured the independence of the results with the mass of the tracer used before conducting the entire experimental campaign. Before injecting the tracer, we ensured that steady-state was reached by measuring the evolution of the outlet mass flow rate over time and checking the value consistency (within a margin of ± 0.1 $kg.h^{-1}$) over three measurements. At steady-state (usually reached after 4 to 5 hours), the tracer was injected just before the kiln entrance, and samples were collected at the outlet at 30-s intervals. The experimental measurement time varied between 11.5 min and 51.5 min depending on the operating conditions. After collection, the samples were weighted to obtain the total mass of the sample. The painted crozets were then sorted and weighed to deduce the mass concentration of the tracer over time and to subsequently calculate the experimental *E(t)* curve. In total, we performed 38 experiments with crozets [34]. *Table 2* presents the range of operating conditions explored.

Table 2: Range of operating conditions explored

Parameter	***Range***
$\dot{M}$ ($kg.h^{-1}$)	1.65 to 6.40
N (RPM)	3.1 - 6 - 9
S (°)	1.5 - 2.9 - 4 - 5
h_{dam} (mm)	13.5 - 23.5 - 33.5
Lifter (-)	NL - SL

$\dot{M}$, N, S and h_{dam} stand for the mass flow rate, rotation speed, kiln slope and dam height, respectively.

3.4 Data treatment and statistical analysis

Data treatment was performed with the matrix calculation software MATLAB (MATLAB 9.4.0.813, MathWorks, USA). Experimental *Pe* and $\bar{t}$ were obtained by fitting *(3)* to experimental *E(t)* curves with the function *nlinfit*. For dimensionless models, we estimated the appropriate coefficients using a multiple linear regression based on the singular value decomposition method (function *fitlm*) after applying a logarithm to the monomial correlations. In terms of statistical analyses, we performed an F-test on the model and a Student's t-test to guarantee the significance of the coefficients.

4. Results and discussion

4.1. Relevance of the methodology

The relevance of the experimental RTD determination methodology for highly non-spherical crozets was assessed before treating the data. *Figure 2* presents the results obtained for three experiments with different behaviors in terms of dispersion and mean residence time (experiments 1, 2 and 3 of *Table 3*). We can observe that the methodology produces RTD curves of the expected shape for a tracer pulse injection. However, some experimental noise must be noted for the most dispersed experiments, related to the limitations of using a solid tracer. The minimal amount of tracer detected is indeed the mass of one single crozet, which can lead to low *E(t)* resolutions in cases where the samples collected are only composed of a handful of particles. The transverse flow regime (rolling or sliding) does not affect the quality of the curves obtained.

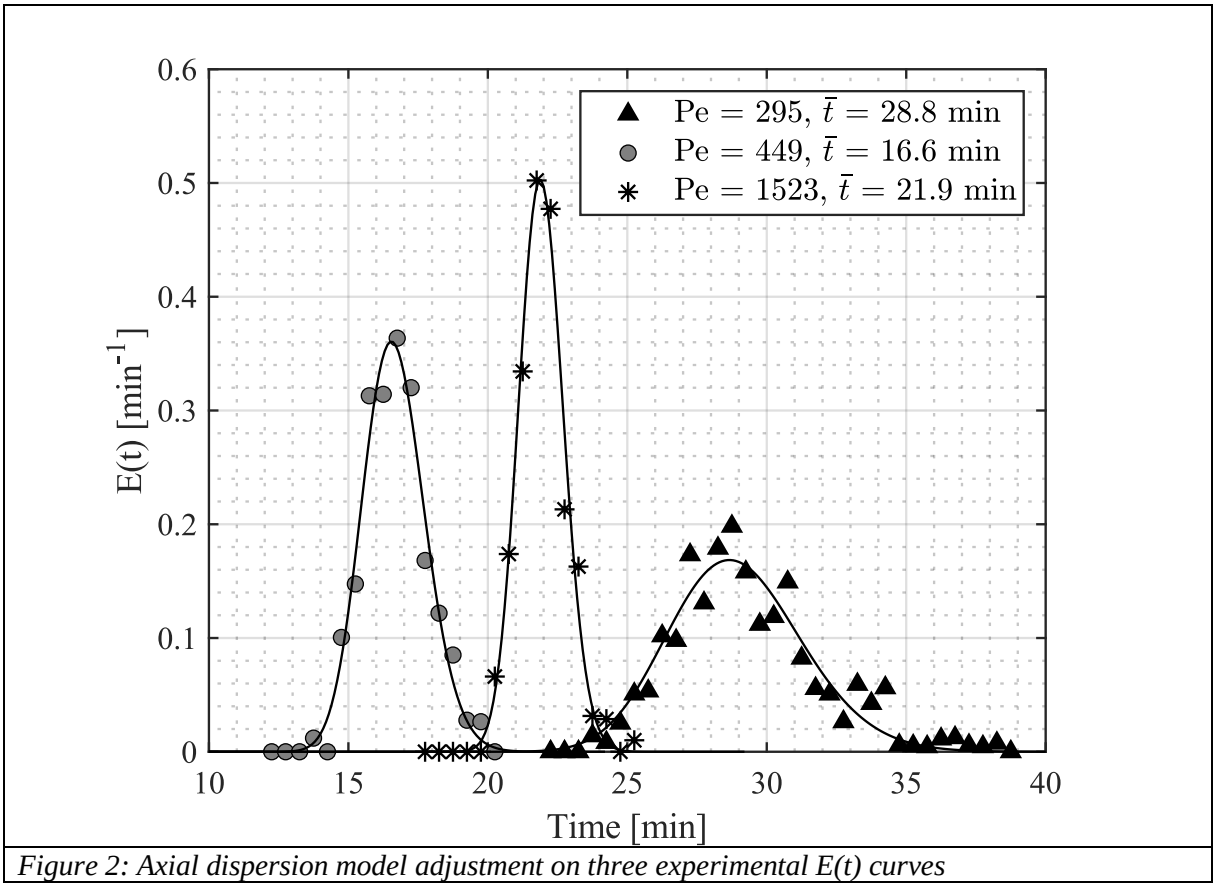

Figure 2: Axial dispersion model adjustment on three experimental E(t) curves

Moreover, the axial dispersion model (represented with solid lines in *Figure 2*) proposes a satisfactory representation of the RTD in terms of mean residence time and axial dispersion since the peak and width of the curves are well fitted over a large range of *Pe* and $\bar{t}$. All the following results are thus presented using this experimental methodology and theoretical background.

4.2. Qualitative influence of the operating conditions on the RTD

We selected 12 conditions (*Table 3*) over the 38 experiments conducted to qualitatively explore the influence of some of the process parameters on the mean residence time $\bar{t}$ and axial dispersion coefficient *D*. As mentioned in *Part 3*, the mass flow rate is manually measured after ensuring a steady-state and is thus not regulated. For this reason, slight differences in mass flow rates may appear in cases in which the value is assumed to be the same when comparing experiments. *Table 4* presents the fitting results of *(3)* obtained for these experiments (*Pe* and $\bar{t}$). In addition, the axial dispersion coefficient *D* is calculated from *(2)* by estimating the mean axial velocity *u* with the kiln length *L* and mean residence time $\bar{t}$.

Table 3: Operating conditions for some of the experimental results presented

Experiment number	***$\dot{M}$ (kg.h^{-1})***	***N (RPM)***	***S (°)***	***h_{dam}***	***Lifter***
1	2.79	3.1	1.5	13.5	NL
2	3.01	6	1.5	33.5	NL
3	3.65	3.1	5	33.5	NL
4	5.33	6	1.5	33.5	NL
5	1.65	6	1.5	33.5	NL
6	2.93	3.1	1.5	23.5	NL
7	2.77	3.1	1.5	33.5	NL
8	2.77	6	1.5	13.5	NL
9	3.14	9	1.5	13.5	NL
10	2.65	3.1	1.5	13.5	SL
11	2.94	6	1.5	13.5	SL
12	2.72	9	1.5	13.5	SL

Table 4: Pe, $\bar{t}$ and D values obtained for the axial dispersion modeling

Experiment number	$\boldsymbol{Pe}$ $(-)$	$\bar{t}$ **(min)**	D $(\mathbf{m^2.s^{-1}})$
1	1523	21.9	1.90E-06
2	295	28.8	7.48E-06

3	449	16.6	8.52E-06
4	643	21.8	4.53E-06
5	188	40.2	8.38E-06
6	2098	28.1	1.07E-06
7	587	40.5	2.67E-06
8	1029	12.7	4.86E-06
9	577	9.1	1.21E-05
10	456	39.0	3.57E-06
11	257	19.6	1.26E-05
12	195	14.4	2.26E-05

4.2.1 Influence of the mass flow rate

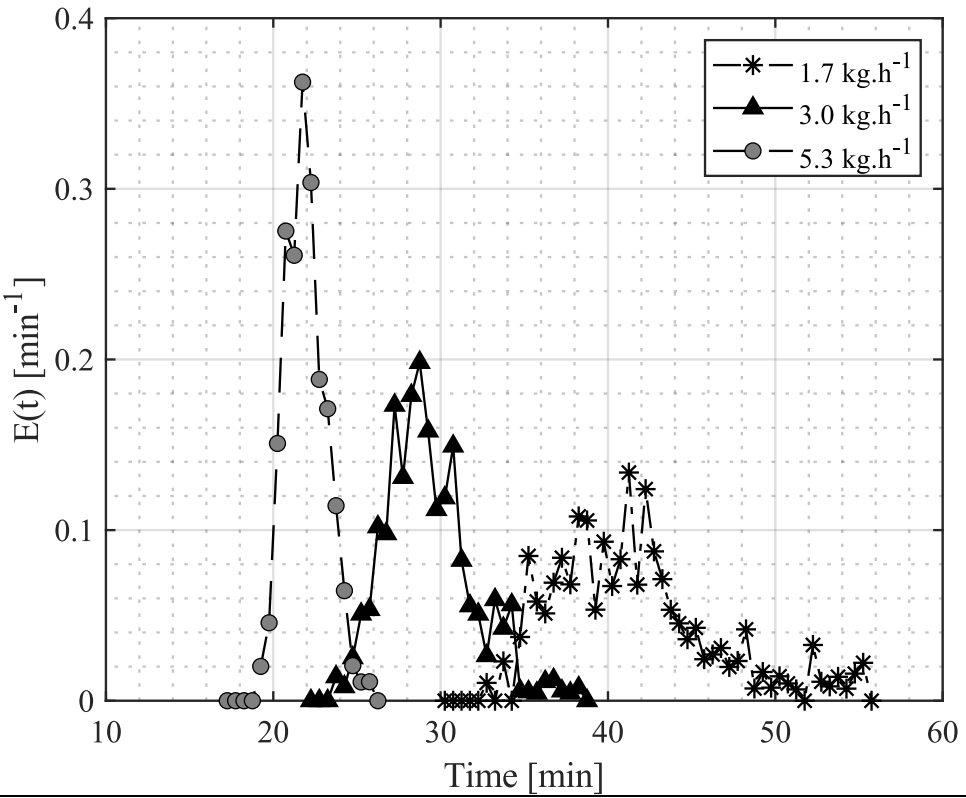

Figure 3: Influence of the mass flow rate on the RTD

The influence of the mass flow rate on the RTD of crozets can be assessed with experiments 2, 4 and 5 (*Figure 3*: Influence of the mass flow rate on the RTD). These experiments were performed without lifters, at N = 6 RPM, h_{dam} = 33.5 mm and S = 1.5°. We observe in *Table 4* that the higher the flow rate is, the lower the residence time and the lower the axial dispersion coefficient will be. The curve flattening and the increase in mean residence time with the decrease in flow rate is qualitatively consistent with previously published results for other solids [19,35]. However, it should be noted that this trend has not been universally found. As an example, Gao et al. [36] reported that while the axial

dispersion coefficient of spheres decreased with increasing feed rates, the coefficient of cylinders and quadrulobes remained almost identical. Recently, Mahdavi et al. [17] also observed that the evolution of the axial coefficient dispersion of 6-mm wood cubes with mass flow rates depended on the rotation speed, with almost identical values of D for mass flow rates of 0.67 and 1.08, and a rotation speed of 3 RPM, followed by large discrepancies at N = 7 RPM (with an increase in D with increasing flow rate), and ultimately similar values at N = 11 RPM. Product and process parameters thus seem to affect the impact of the mass flow rate on D.

4.2.2 Influence of the dam height

Experiments 1, 6 and 7 are used to qualitatively observe the influence of the dam height on the RTD curves (*Figure 4*). These experiments correspond to the following working conditions: no lifters, N = 6 RPM, S = 1.5°, and $\dot{M}$ approximately equal to 2.8 kg.h^{-1} (between 2.77 and 2.93). The increase in dam height translates into an increase in the amount of solid retained inside the kiln, which promotes dispersion and longer residence time. It, however, must be noted that the identification reveals a dispersion somewhat similar for h_{dam} = 13.5 mm and 23.5 mm. This observation is relatively consistent with the findings of Bongo Njeng et al. [37]. The authors indeed found that regardless of the lifter used (straight or rectangular) in the cases of rice and sand, the axial dispersion coefficient was quite similar with increasing dam height. The only difference is the sharp increase in D for the largest dam height, which might be related to the hold-up of the kiln. The hold-up is indeed much higher with the last dam than with the two others, enhancing dispersion.

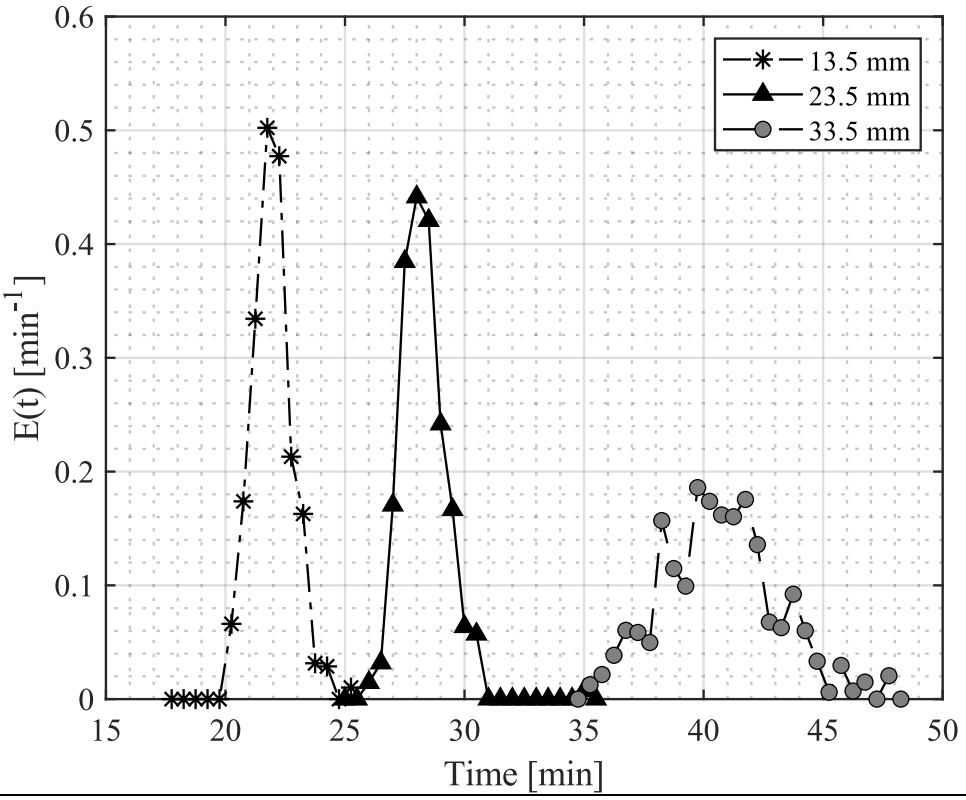

Figure 4: Influence of the dam height on the RTD

4.2.3 Influence of the rotation speed

The influence of *N* can be assessed by observing the results achieved with experiments 1, 8 and 9 and presented in *Figure 5*. Looking at the values of *D* and $\bar{t}$ in *Table 4*, we can see that $\bar{t}$ decreases with increasing *N*, while *D* increases. The decrease of the mean residence time with an increasing rotation speed was already observed by Bongo Njeng et al. in the same apparatus without and with lifters when studying beech chip flow in a somewhat larger kiln, as well as the increase of *D* in the same experimental conditions. Recently, Mahdavi et al. [17] obtained the same behavior (decrease in $\bar{t}$ and increase in *D* with increasing *N*) at moderate slopes (between 2 and 4°) and rotation speeds (between 3 to 7 RPM) for 6-mm wood cubes.

Sherritt et al. [25] observed that the dependence of the axial dispersion coefficient on the drum rotation speed is intimately related to the rotation regime achieved. In a slumping regime, the coefficient decreases with *N*, whereas in the case of rolling and cataracting regimes, it increases. More precisely, he found that *D* approximately depends on $N^{0.5}$ for rolling and *N* for cataracting. The increase of *D* observed here with increasing *N* is also consistent with these observations. It should be noted that a decrease of *D* with *N* was also observed by Mahdavi et al. for *N* higher than 7 RPM and slopes of 3 and 4°. They attributed this evolution to a change in regime (slumping), according to the observations of Sherritt.

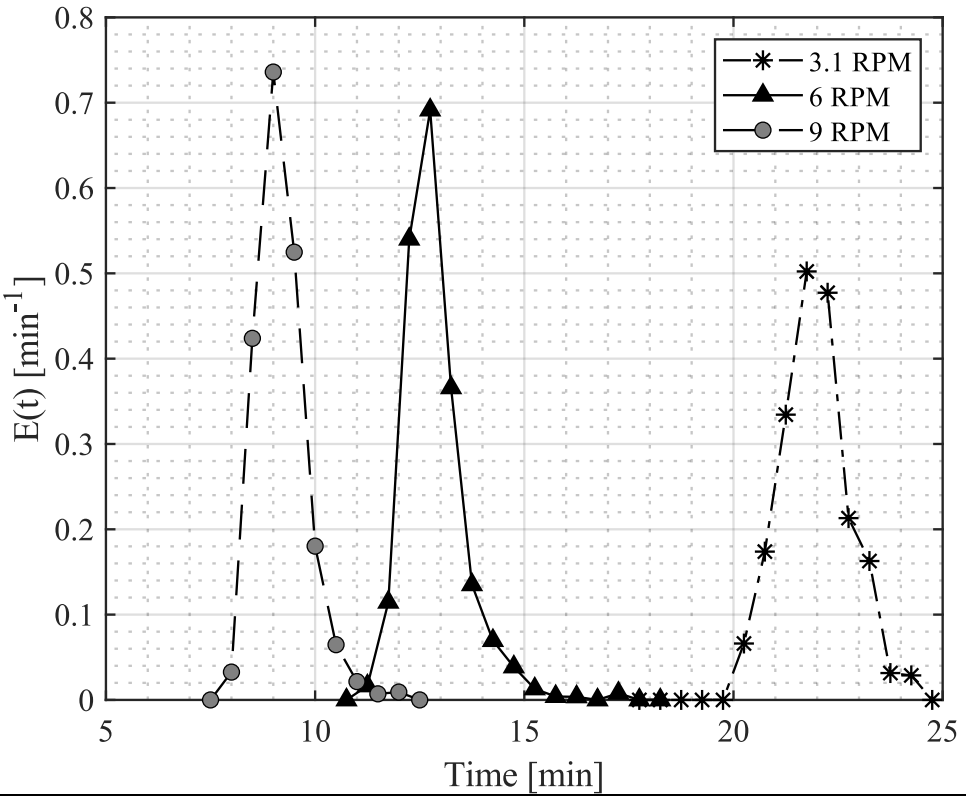

Figure 5: Influence of the rotation speed on the RTD

4.2.4 Influence of the lifters

The influence of the lifters can be observed by comparing Experiments 10, 11 and 12 with Experiments 1, 8 and 9 (*Figure 6*). In these experiments, $\dot{M}$ approximately equals 2.8 kg.h^{-1}, h_{dam} is 33.5 mm and S = 1.5°. Straight lifters have a clear impact as they systematically increase D and $\bar{t}$ at constant N. The explanation of this behavior probably lies in the retention capacity of the lifters. Solid particles are more likely to be kept inside the lifters and then cascade later, creating a delay in the axial transportation and promoting dispersion. It should be noted that comparing the influence of two types of lifters is somewhat more complex than this straightforward explanation since the discharge rate of the lifters will influence the global hydrodynamic behavior.

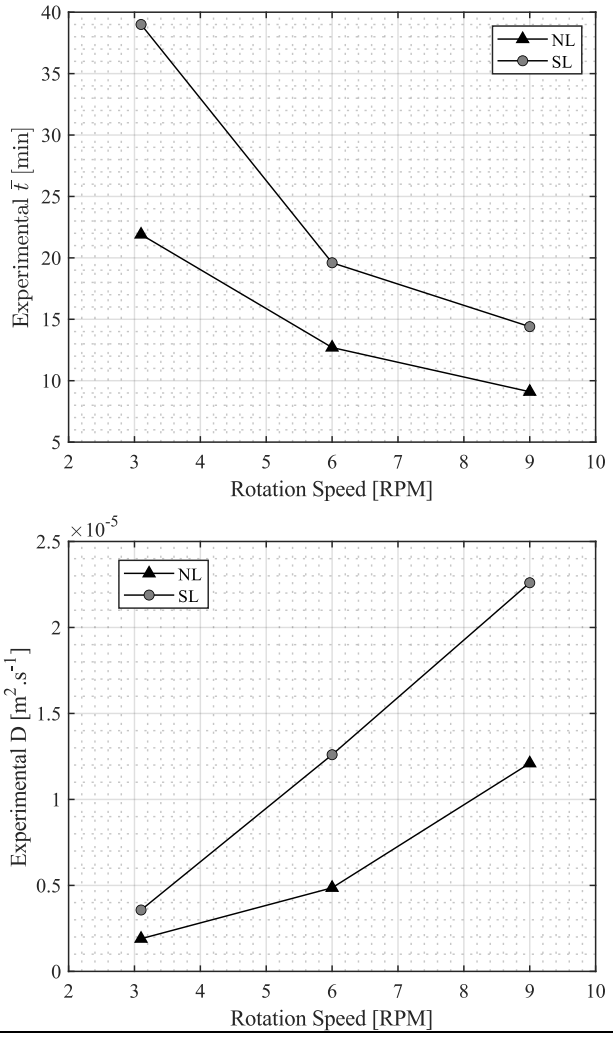

Figure 6: Influence of the straight lifter on $\bar{t}$ and D for increasing rotation speed

4.3. Dimensional analysis modeling

4.3.1 Description of the models proposed by Bongo Njeng et al.

Dimensional analysis is frequently used in chemical engineering since it offers a way to accurately model complex phenomena through semi-empirical models, mostly of monomial shape. This approach is still extensively used to simply predict properties of interest (characteristic diameters for bifluid spray drying [38], gas-liquid mass transfer coefficients in stirred tanks [39], mixing times in a soft elastic reactor [40], etc.) from dimensionless numbers. The dimensionless correlations obtained have a strong physical meaning by using well-known numbers such as the Reynolds number, Weber number, etc.

Regarding the hydrodynamics inside rotary kilns, several dimensionless correlations predicting *D* and $\bar{t}$ can be found in the literature [41–44]. Nonetheless, they generally do not include all the parameters (operating or physical) that can influence these hydrodynamic parameters. Based on a rigorous dimensional analysis methodology and a consistent set of experiments, Bongo Njeng et al. proposed models that allowed the prediction of $\bar{t}$, *D* and the bed height based on the application of the Vashy-Buckingham theorem. *(4)* and *(5)* present the shape of the equations proposed by the authors to estimate $\bar{t}$ and *D*, respectively. *Table 5* presents the coefficients identified.

$$\bar{t} = k\sqrt{\frac{L}{g}}\left(\frac{N^2 d_i}{g}\right)^{\alpha}\left(\frac{d_{exit}}{d_i}\right)^{\beta}\left(\frac{\theta_p}{S}\right)^{\gamma}\left(\frac{\dot{M}}{\rho_{bulk}{d_i}^2\sqrt{gL}}\right)^{\delta}\left(\frac{4S_{lift}}{\pi{d_i}^2}\right)^{\varepsilon}\left(\frac{\rho_{bulk}}{\rho_{tapped}}\right)^{\delta}\left(\frac{L}{d_i}\right)^{\eta} \quad (4)$$

$$D = k\sqrt{D_i^2 gL}\left(\frac{N^2 d_i}{g}\right)^{\alpha}\left(\frac{d_p}{d_i}\right)^{\beta}(S)^{\gamma}\left(\frac{\dot{M}}{\rho_{bulk}{d_i}^2\sqrt{gL}}\right)^{\delta}\left(\frac{4S_{lift}}{\pi{d_i}^2}\right)^{\varepsilon}\left(\frac{\rho_{bulk}}{\rho_{tapped}}\right)^{\zeta}\left(\frac{L}{d_i}\right)^{\eta} \quad (5)$$

Some of the dimensionless numbers used in these correlations are of particular interest for physical interpretation:

- $\frac{N^2 d_i}{g}$ is also called the Froude number, and compares centrifugal forces to gravity. It is useful for characterizing the particle bed motion [32];
- $\frac{\rho_{bulk}}{\rho_{tapped}}$ is the multiplicative inverse of the Hausner ratio that quantifies the flowability aptitude of a powder;
- $\frac{\dot{M}}{\rho_{bulk}{d_i}^2\sqrt{gL}}$ encompasses the mass flow rate influence;
- $\frac{4S_{lift}}{\pi{d_i}^2}$ estimates the fraction of the tube cross-section uncovered by particles when using lifters.

The exit diameter d_{exit} is calculated from the internal kiln diameter d_i and the dam diameter h_{dam} according to the following equation (*(6)*):

$$d_{exit} = d_i - 2.h_{dam} \quad (6)$$

S_{lift} is the area uncovered by particles in a horizontal position and can be calculated with *(7)*.

$$S_{lift} = \pi.\frac{{d_i}^2}{4} - \frac{n_{lift} - 1}{2}.\frac{V}{L_{kiln}} \quad (7)$$

V denotes the volume of solids retained inside the lifters in a horizontal position and is estimated from the repose angle according to the equations presented in [45].

Table 5: Coefficients obtained by Bongo Njeng et al.

	k	α	β	γ	δ	ε	δ	η
$\bar{t}$ **(s)**	0.0252	- 0.4422	-0.3597	0.9276	-0.1130	-8.8835	-2.4641	1.1
D ($m^2.s^{-1}$)	$1.52*10^{-4}$	0.7483	0.2996	1.9859	-0.4511	1.2185	5.5513	0

2.3.2 Adequation of the models for the crozets

We first used the models to predict the values of $\bar{t}$ and D from our 38 experimental conditions. The characteristic crozet diameter considered for the calculation is the diameter corresponding to a sphere of equivalent surface, calculated with *(8)*:

$$d_p = 6.\frac{V_p}{A_p} \qquad (8)$$

where V_p and A_p stand for the particle volume and area, respectively. *Figure 7* shows the results predicted for the mean residence time, where solid lines represent ± 20% intervals. Seventeen experiments out of 38 were greatly overpredicted (prediction outside the 20% interval). When looking at the dimensionless number values calculated for these experiments, we can observe several interesting facts:

- $\frac{\rho_{bulk}}{\rho_{tapped}}$ is lower than the lowest values used for the model establishment, meaning that the crozet experiments are slightly out-of-bounds in terms of $\frac{\rho_{bulk}}{\rho_{tapped}}$ values for strict correlation application;
- 16/17 of the overpredicted results are obtained with $\frac{4S_{lift}}{\pi {d_i}^2}$ = 1 (no lifter condition) and 14/17 with $\frac{\theta_p}{S}$ = 18.6. The model proposed by Bongo Njeng et al. thus does not predict accurate mean residence time with this combination of parameters (specific angle of repose and no lifters).

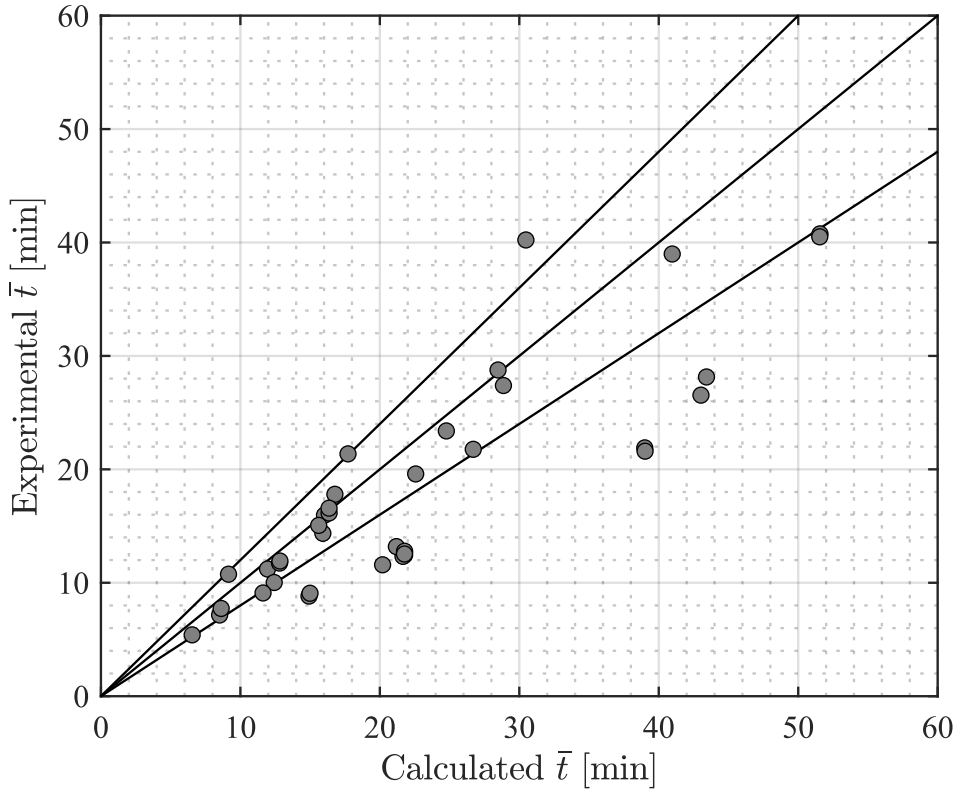

Figure 7: $\bar{t}$ prediction for crozets (Bongo Njeng et al. model)

Figure 8 presents the axial dispersion coefficient prediction using the model proposed in [21], with solid lines representing deviations at ± 30%. Only seven experiments were predicted within the 30% range. Some remarks can be made about the dimensionless number values calculated with our experimental conditions:

- $\frac{d_p}{d_i}$ in the dataset of this study is actually higher than the maximal value encountered in the previous set of experiments (more than 20%);
- $\frac{\rho_{bulk}}{\rho_{tapped}}$ is also slightly out-of-bounds (likewise, the mean residence time correlation);
- Low *S* values were barely explored with the previous experimental dataset, whereas 20 experiments out of the 38 for crozets were obtained with S = 1.5° (low slope).

All these remarks thus highlight the need to re-identify the models using this study's experimental data. This re-identification will thus offer correlations with a broader range of validity and better accuracy.

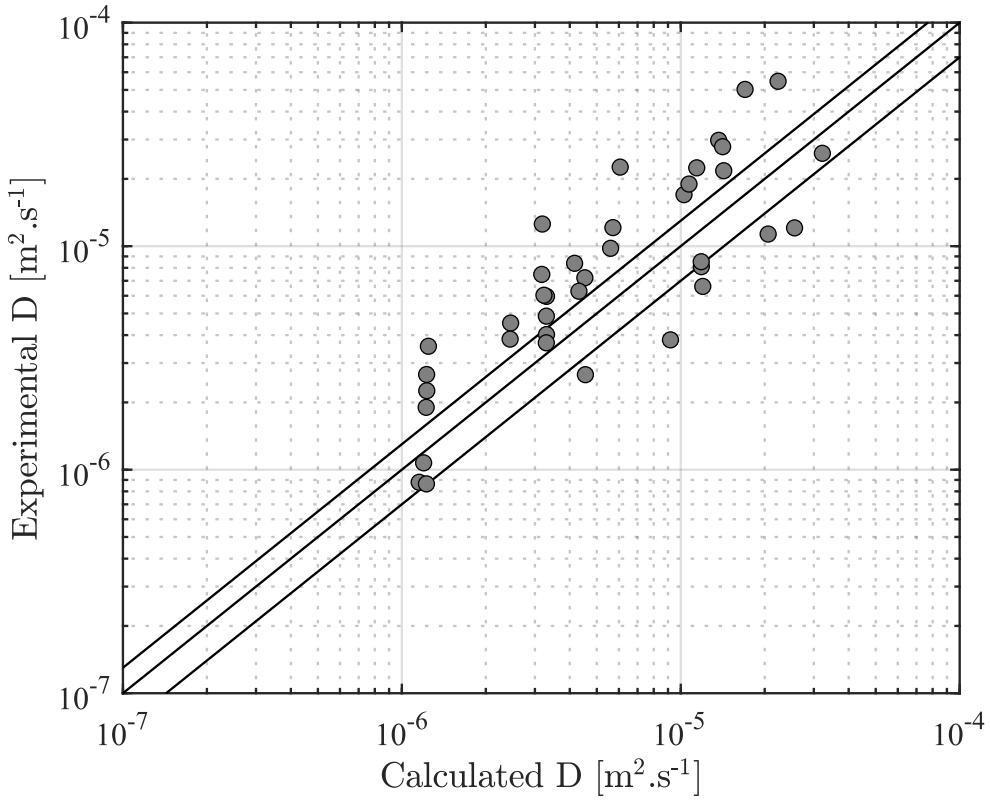

Figure 8: D prediction for crozets (Bongo Njeng et al. model)

2.3.3 Re-identification of the models

The dimensionless models were re-identified to better account for crozet properties and to propose more generic correlations. To that extent, the identification methodology for experimental $\bar{t}$ and *D* described in Section *3.4* was also used on the raw data from Bongo Njeng et al., ensuring consistent data treatment. Adding the 38 results of this study [34] to the 122 already performed by Bongo Njeng et al. [46–48] thus gave a pool of 160 experimental results on which the dimensionless model identification was performed. The experiments made by Bongo Njeng et al. with sand and rice were performed in the kiln used in this study. Beech was studied in another kiln that is extensively described elsewhere [21].

We also recalculated the characteristic diameters for sand, rice and beech using the definition introduced by *(8)*. For this diameter calculation, we considered sand as a sphere, rice as a cylinder, and beech as a parallelepipedal rectangle. The equivalent diameters were then calculated using the conventional definitions of surface and volume for these geometries and the numerical values of *Table 1*. This homogenization also simplifies the application of the newly identified correlations to geometries other than the ones considered in this study.

All the dimensionless numbers proposed by the dimensionless analysis were *a priori* considered for the re-identification. The statistical analysis described in Section *3.4* then allowed some simplifications when the coefficients' p-values were higher than 0.05. *Table 6* presents the parameters identified with the complete set of experiments for $\bar{t}$ and *D*, while *Table 7* shows the validity range of the new equations. The parity plots for these models are shown in *Figure 9* and *Figure 10*. For the mean residence time model, the logarithm multilinear regression gave $R^2 = 0.93$ and a Root-Mean-Square Error (RMSE) of 0.142, whereas in the case of *D*, $R^2 = 0.78$ and RMSE = 0.467. No value for

the $\frac{L}{d_i}$ coefficient (η in *(4)*) was assumed *a priori*, unlike the previous identification proposed by Bongo Njeng et al. In addition, the inverse Hausner ratio did not significantly impact $\bar{t}$ in this study and was thus removed after prior identification.

Table 6: Re-identified coefficients

	k	α	β	γ	δ	ε	δ	η
$\bar{t}$ **(s)**	$1.0831*10^{-10}$	-0.3951	-0.5994	0.8426	-0.16562	-10.320	0	7.635
D ($m^2.s^{-1}$)	$1.0985*10^{-5}$	0.8749	0.4824	1.3842	-0.7874	-39.3	-6.750	0

Table 7: Range of validity of the correlations

Dimensionless number	Range (Bongo Njeng et al.)	Range (this study)
$\frac{N^2 d_i}{g}$	1.15e-05 - 4.13e-04	1.15e-05 - 4.13e-04
$\frac{d_{exit}}{d_i}$	0.34 – 1.00	0.34- 1.00
$\frac{\theta_p}{S}$	7.20 – 42.00	5.58 – 42.00
$\frac{\dot{M}}{\rho_{bulk} {d_i}^2 \sqrt{gL}}$	2.87e-06 - 2.86e-05	2.87e-06 - 5.93e-05
$\frac{4S_{lift}}{\pi {d_i}^2}$	0.977 - 1	0.977 - 1
$\frac{\rho_{bulk}}{\rho_{tapped}}$	0.916 - 0.958	0.873 - 0.958
$\frac{L}{d_i}$	19.25 - 20	19.25 - 20
$\frac{d_p}{d_i}$	5.40e-03 – 3.19 e-02	5.40e-03 – 3.45 e-02
S	1.00 – 5.00	1.00 – 5.00

Several differences between the mean residence time models can be observed when comparing the old coefficients (*Table 5*) with the ones identified in this study (*Table 6*). First, the inverse Hausner ratio was not found to significantly impact the new model and was thus removed from the equation. Then, unlike the study of Bongo Njeng et al., η was not imposed. As a result, the $\frac{L}{d_i}$ dimensionless number was found to affect the residence time more than expected with the previous model. The other identified coefficients are on the same order of magnitude as the previous ones, giving confidence in the robustness of this enhanced model.

For the axial dispersion model, some comparisons can also be drawn. $\frac{L}{d_i}$ does not significantly affect the new axial dispersion model. This non-significance might mean that the flow is well established over the dimensionless lengths studied and $\frac{L}{d_i}$ is thus not expected to affect the axial dispersion coefficient. While most of the new coefficients remain on the same order of magnitude as the previous ones, two differences are particularly noticeable. ε and δ indeed have the values of the opposite sign

compared to the first version of the model, indicating that the model predicts an influence of $\frac{4S_{lift}}{\pi {d_i}^2}$ and $\frac{\rho_{bulk}}{\rho_{tapped}}$ on *D* opposite to what Bongo Njeng et al. found. The restricted range of variation associated with these numbers and their order of magnitude close to unity (*Table 7*) might be the reasons for these changes.

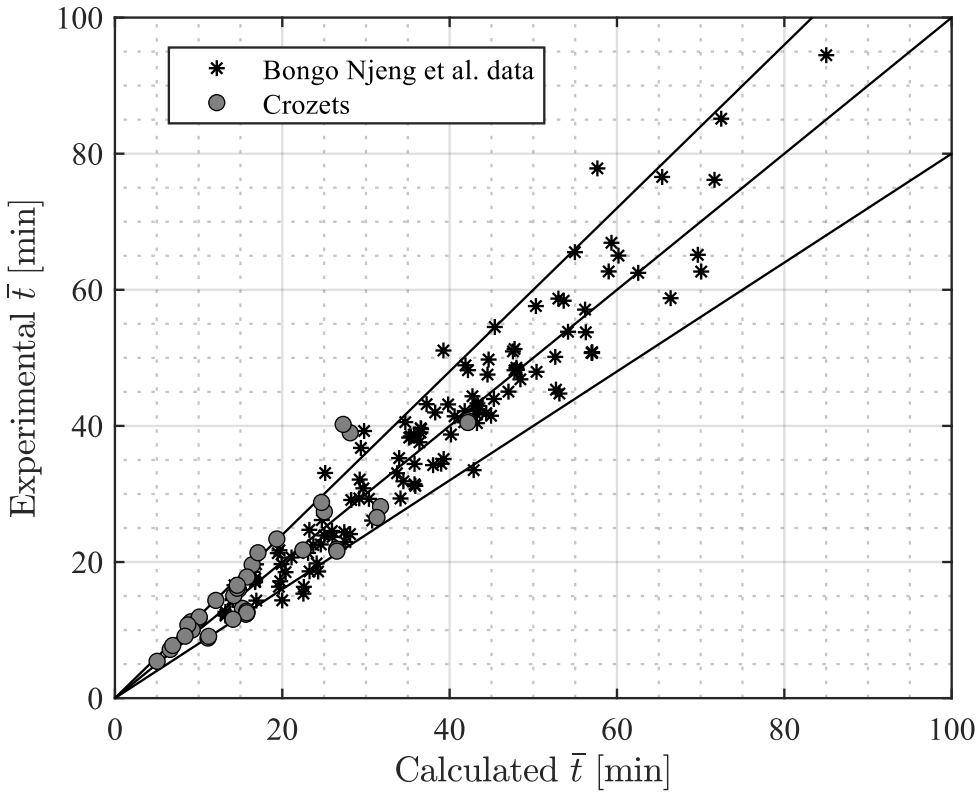

Figure 9: Mean residence time model re-identification

These models significantly improved the overall prediction capability for crozets. We can observe in *Figure 9* that for $\bar{t}$, 6/38 experiments are now underpredicted (higher than 20% of deviation). When we consider a 30% range, this number falls to 2/38, proving the satisfactory accuracy of this model.

D is substantially more complex to seize as it encompasses a diversity of physical phenomena. *Figure 10*: Axial dispersion model re-identification presents the parity plot obtained for our model that predicts *D*. Nineteen out of 38 experiments are not predicted within the 30% interval, and 4/38 when considering a 60% interval. While not perfect, the model still allows us to obtain reasonable estimations of the axial dispersion coefficient.

It should be mentioned that the shape of the equation itself can be questioned. The Vashy-Buckingham theorem makes it possible to build a relevant set of dimensionless numbers. The theorem, however, does not state the shape of the equation correlating these numbers. A monomial form is conventionally assumed for these correlations but might not be the most suited mathematical shape depending on the phenomenon considered. Recent studies [38,49] showed that combining dimensional analysis with machine learning can help to find more accurate equations than those found using the conventional approach. Moreover, the contribution of each parameter/dimensionless parameter is very likely to vary depending on the hydrodynamic regime considered (sliding, slumping, rolling, etc.). More robust axial

dispersion modeling should consider this fact and propose a different set of correlations depending on the observed regime.

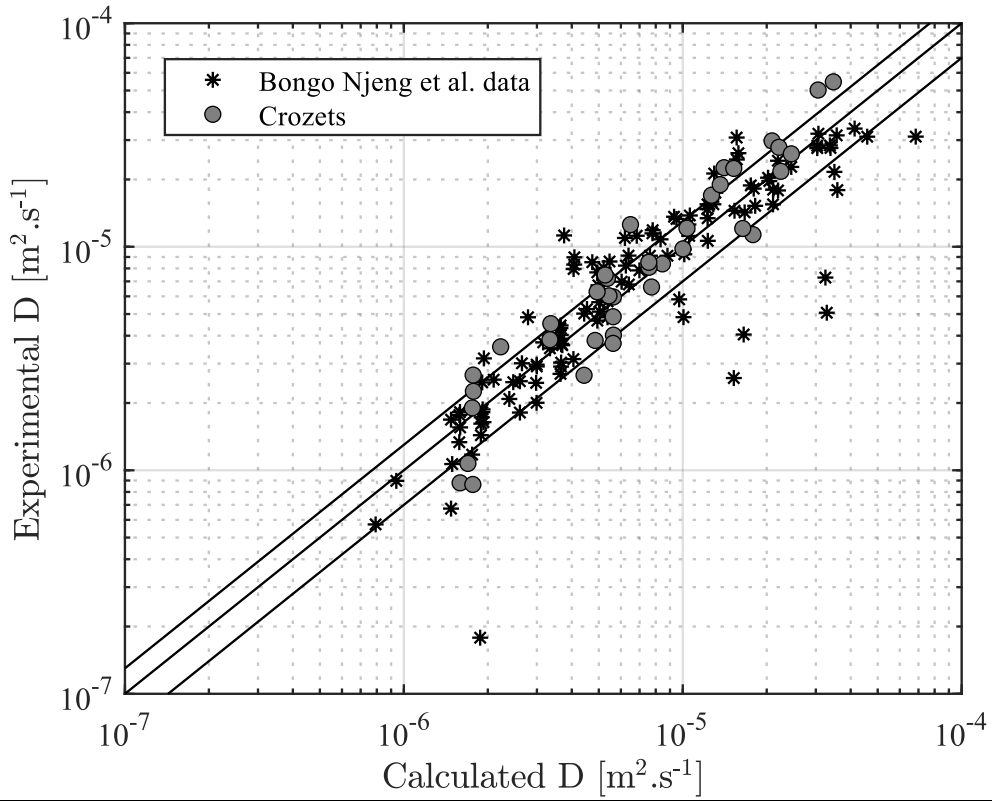

Figure 10: Axial dispersion model re-identification

Conclusion

Due to the diversity of products handled by rotary kilns, relevant generic hydrodynamic and thermal models must be provided to offer quick and reliable estimations of parameters of interest such as the mean residence time, the axial dispersion coefficient and the heat transfer coefficient. This study first focused on the experimental behavior of a highly non-spherical and rather large granular product: the crozet. The experimental study showed that the conventional axial dispersion model with open-open boundary conditions offered an adequate representation of the residence time distribution of this product inside a rotary kiln, and that the observed behavior was qualitatively coherent with observations made in the literature.

The robustness of the models proposed by Bongo Njeng et al. was subsequently tested on this product. Almost half of the experimental mean residence times were not reasonably estimated, whereas the axial dispersion prediction generally failed. Some dimensionless numbers were outside the range in which the original correlation was established, meaning that the equations proposed by Bongo Njeng et al. were not strictly applicable to our experiments, which can explain these discrepancies. The dimensionless models for the mean residence time and axial dispersion were thus re-identified, with the help of a statistical analysis that allowed some simplifications. The re-identified models offered a

more satisfactory prediction of both the mean residence time and the axial dispersion coefficient for crozets. Overall, they reasonably predicted these values over the whole range of experiments considered. In addition to providing new experiments to feed the models, further exploration of dimensionless modeling of these hydrodynamic properties should consider finding new shapes for the correlations or better account for the specificities of each hydrodynamic regime.

Nomenclature

A_p	Particle surface (m²)
C	Dimensionless tracer concentration (-)
D	Axial dispersion coefficient ($m^2.s^{-1}$)
d_{exit}	Effective exit kiln diameter (m)
d_i	Internal kiln diameter (m)
d_p	Particle equivalent diameter (m)
g	Gravitational acceleration constant ($m.s^{-2}$)
h_{dam}	Dam height (m)
L	Kiln length (m)
$\dot{M}$	Material mass flow rate ($kg.s^{-3}$)
N	Kiln rotation speed (rotations per second)
R^2	Pearson linear determination coefficient (-)
S	Kiln slope (°)
S_{lift}	Area covered by solid particles in a lifter in horizontal position (m²)
$\bar{t}$	Mean residence time (s)
u	Mean axial velocity ($m.s^{-1}$)
V_p	Particle volume (m^3)

Greek letters

ρ_{bulk}	Bulk density ($kg.m^{-3}$)
ρ_{tapped}	Tapped density ($kg.m^{-3}$)
θ	Dimensionless time (-)
θ_p	Angle of repose (°)
ζ	Dimensionless axial distance (-)

Abbreviations

DEM	Discrete Element Method
RMSE	Root-Mean-Square Error
RTD	Residence Time Distribution

Data availability

The experimental data (including raw experimental results, product and kiln properties) are available in the dataverse, “Rotary kilns and drums”, on the French national repository, Recherche Data Gouv (https://entrepot.recherche.data.gouv.fr/dataverse/rkd), and the corresponding DOIs are quoted in the article.

The Associated Data Management Plan is published in French [50].

Acknowledgments

The authors would like to thank Maud LESCROART and Paul FOURRE for the experiments they conducted as part of an engineering project carried out at AgroParisTech, as well as Clément HAUSTANT, technician at Cnam, for his technical support.

References

[1] B.-J.R. Mungyeko Bisulandu, F. Huchet, Rotary kiln process: An overview of physical mechanisms, models and applications, Applied Thermal Engineering. 221 (2023) 119637. https://doi.org/10.1016/j.applthermaleng.2022.119637.
[2] J. Lasek, K. Głód, K. Słowik, A. Cygan, Y.-H. Li, Static and dynamic characteristics of rotary kiln reactor during processing of biomass and municipal solid waste, Powder Technology. 404 (2022) 117476. https://doi.org/10.1016/j.powtec.2022.117476.
[3] F. Proch, K. Bauerbach, P. Grammenoudis, Development of an up-scalable rotary kiln design for the pyrolysis of waste tyres, Chemical Engineering Science. 238 (2021) 116573. https://doi.org/10.1016/j.ces.2021.116573.
[4] E. Yazdani, S.H. Hashemabadi, A. Taghizadeh, Study of waste tire pyrolysis in a rotary kiln reactor in a wide range of pyrolysis temperature, Waste Management. 85 (2019) 195–201. https://doi.org/10.1016/j.wasman.2018.12.020.
[5] X. Liu, L. Duan, Y. Duan, L. Li, Z. Sun, G. Sun, Improved fuel conversion through oxygen carrier aided combustion during incineration of biomass-based solid waste in a rotary kiln, Fuel. 331 (2023) 125714. https://doi.org/10.1016/j.fuel.2022.125714.
[6] E. Hu, Y. Tian, Y. Yang, C. Dai, M. Li, C. Li, S. Shao, Pyrolysis behaviors of corn stover in new two-stage rotary kiln with baffle, Journal of Analytical and Applied Pyrolysis. 161 (2022) 105398. https://doi.org/10.1016/j.jaap.2021.105398.
[7] J.D.O. da Silva, A. Wisniewski, I.S.C. Carregosa, W.R. da Silva, A.K. de S. Abud, A.M. de Oliveira Júnior, Thermovalorization of acerola industrial waste by pyrolysis in a continuous rotary kiln reactor, Journal of Analytical and Applied Pyrolysis. 161 (2022) 105373. https://doi.org/10.1016/j.jaap.2021.105373.
[8] M. Pichler, B. Haddadi, C. Jordan, H. Norouzi, M. Harasek, Dataset for the simulated biomass pyrolysis in rotary kilns with varying particle residence time distributions, Data in Brief. 39 (2021) 107603. https://doi.org/10.1016/j.dib.2021.107603.
[9] M. Adepu, S. Chen, Y. Jiao, A. Gel, H. Emady, Wall to particle bed contact conduction heat transfer in a rotary drum using DEM, Comp. Part. Mech. 8 (2021) 589–599. https://doi.org/10.1007/s40571-020-00356-z.

[10] E. Ardalani, B. Yohannes, W.G. Borghard, B.J. Glasser, A.M. Cuitiño, DEM analysis of the thermal treatment of granular materials in a rotary drum equipped with baffles, Chemical Engineering Science. 251 (2022) 117476. https://doi.org/10.1016/j.ces.2022.117476.
[11] L. Zhang, Z. Jiang, J. Mellmann, F. Weigler, F. Herz, A. Bück, E. Tsotsas, Influence of the number of flights on the dilute phase ratio in flighted rotating drums by PTV measurements and DEM simulations, Particuology. 56 (2021) 171–182. https://doi.org/10.1016/j.partic.2020.09.010.
[12] G. Xu, Y. Zhang, X. Yang, G. Chen, B. Jin, Effect of drum structure on particle mixing behavior based on DEM method, Particuology. 74 (2023) 74–91. https://doi.org/10.1016/j.partic.2022.05.008.
[13] M. Hellou, F. Lominé, I. Benhsine, Y. Roques, Theoretical description of the motion of a particle in rotary dryer, Can. J. Chem. Eng. 97 (2019) 103–114. https://doi.org/10.1002/cjce.23213.
[14] Z. Zhang, Y. Wu, H. Li, X. Li, X. Gao, A simple step-change method to determine mean residence time in rotary kiln and a predictive model at low inclination, Powder Technology. 333 (2018) 30–37. https://doi.org/10.1016/j.powtec.2018.04.002.
[15] I.Y. Chen, S. Navodia, B. Yohannes, L. Nordeck, B. Machado, E. Ardalani, W.G. Borghard, B.J. Glasser, A.M. Cuitiño, Flow of a moderately cohesive FCC catalyst in two pilot-scale rotary calciners: Residence time distribution and bed depth measurements with and without dams, Chemical Engineering Science. 230 (2021) 116211. https://doi.org/10.1016/j.ces.2020.116211.
[16] J. Priessen, T. Kreutzer, G. Irgat, M. Behrens, H.J. Schultz, Solid flow in rotary drums with sectional internals: an experimental investigation, Chem. Eng. Technol. 44 (2021) 300–309. https://doi.org/10.1002/ceat.202000148.
[17] S. Mahdavy, H.R. Norouzi, C. Jordan, B. Haddadi, M. Harasek, Residence Time Distribution of non-spherical particles in a continuous rotary drum, Processes. 10 (2022) 1069. https://doi.org/10.3390/pr10061069.
[18] J. Priessen, F. Barths, M. Behrens, H.J. Schultz, The length of axially segmented lifters in flighted rotary drums: influence on solid transport, Drying Technology. 40 (2022) 3003–3020. https://doi.org/10.1080/07373937.2021.1995408.
[19] A.S. Bongo Njeng, S. Vitu, M. Clausse, J.-L. Dirion, M. Debacq, Effect of lifter shape and operating parameters on the flow of materials in a pilot rotary kiln: Part I. Experimental RTD and axial dispersion study, Powder Technology. 269 (2015) 554–565. https://doi.org/10.1016/j.powtec.2014.03.066.
[20] A.S. Bongo Njeng, S. Vitu, M. Clausse, J.-L. Dirion, M. Debacq, Effect of lifter shape and operating parameters on the flow of materials in a pilot rotary kiln: Part II. Experimental hold-up and mean residence time modeling, Powder Technology. 269 (2015) 566–576. https://doi.org/10.1016/j.powtec.2014.05.070.
[21] A.S. Bongo Njeng, S. Vitu, M. Clausse, J.-L. Dirion, M. Debacq, Effect of lifter shape and operating parameters on the flow of materials in a pilot rotary kiln: Part III. Up-scaling considerations and segregation analysis, Powder Technology. 297 (2016) 415–428. https://doi.org/10.1016/j.powtec.2016.04.052.
[22] A.S. Bongo Njeng, S. Vitu, M. Clausse, J.-L. Dirion, M. Debacq, Wall-to-solid heat transfer coefficient in flighted rotary kilns: Experimental determination and modeling, Experimental Thermal and Fluid Science. 91 (2018) 197–213. https://doi.org/10.1016/j.expthermflusci.2017.10.024.
[23] Y. Gao, F.J. Muzzio, M.G. Ierapetritou, A review of the Residence Time Distribution (RTD) applications in solid unit operations, Powder Technology. 228 (2012) 416–423. https://doi.org/10.1016/j.powtec.2012.05.060.
[24] O.S. Sudah, A.W. Chester, J.A. Kowalski, J.W. Beeckman, F.J. Muzzio, Quantitative characterization of mixing processes in rotary calciners, Powder Technology. 126 (2002) 166–173. https://doi.org/10.1016/S0032-5910(02)00009-8.
[25] R.G. Sherritt, J. Chaouki, A.K. Mehrotra, L.A. Behie, Axial dispersion in the three-dimensional mixing of particles in a rotating drum reactor, Chemical Engineering Science. 58 (2003) 401–415. https://doi.org/10.1016/S0009-2509(02)00551-1.
[26] O. Levenspiel, Chemical reaction engineering, 3rd Edition, Wiley, 1999.
[27] A.S. Bongo Njeng, S. Vitu, M. Clausse, J.-L. Dirion, M. Debacq, Sand, Recherche Data Gouv (2023). https://doi.org/10.57745/PZTZ7Y.

[28] A.S. Bongo Njeng, S. Vitu, M. Clausse, J.-L. Dirion, M. Debacq, Broken rice, Recherche Data Gouv (2023). https://doi.org/10.57745/PMC2QZ.
[29] A.S. Bongo Njeng, S. Vitu, M. Clausse, J.-L. Dirion, M. Debacq, Beech chips, Recherche Data Gouv (2023). https://doi.org/10.57745/KOVF5B.
[30] K. Lachin, A. Doche, S. Vitu, M. Debacq, Crozets, Recherche Data Gouv (2023). https://doi.org/10.57745/WLTDBM.
[31] P. Thammavong, M. Debacq, S. Vitu, M. Dupoizat, Experimental Apparatus for Studying Heat Transfer in Externally Heated Rotary Kilns, Chemical Engineering & Technology. 34 (2011) 707–717. https://doi.org/10.1002/ceat.201000391.
[32] J. Mellmann, The transverse motion of solids in rotating cylinders-forms of motion and transition behavior, Powder Technology. 118 (2001) 251–270. https://doi.org/10.1016/S0032-5910(00)00402-2.
[33] M. Debacq, S. Vitu, K. Lachin, A.S. Bongo Njeng, J.-L. Dirion, M. Clausse, Kilns specifications, Recherche Data Gouv (2023). https://doi.org/10.57745/NEAJWN.
[34] K. Lachin, A. Doche, S. Vitu, M. Debacq, Residence Time Distribution - kiln 1 - crozets, Recherche Data Gouv (2023). https://doi.org/10.57745/A0KSMH.
[35] M. Hehl, H. Kroger, H. Helmrich, K. Schugerl, Longitudinal mixing in horizontal rotary drum reactors, Powder Technology. 20 (1978) 29–37. https://doi.org/10.1016/0032-5910(78)80005-9.
[36] Y. Gao, B.J. Glasser, M.G. Ierapetritou, A. Cuitino, F.J. Muzzio, J.W. Beeckman, N.A. Fassbender, W.G. Borghard, Measurement of residence time distribution in a rotary calciner, AIChE Journal. 59 (2013) 4068–4076. https://doi.org/10.1002/aic.14175.
[37] A.S. Bongo Njeng, Experimental study and modeling of hydrodynamic and heating characteristics of flighted rotary kilns, PhD manuscript, Ecole nationale des Mines d'Albi-Carmaux, 2015. http://www.theses.fr/2015EMAC0009.
[38] K. Lachin, M. Niane, M. Person, J. Mazet, G. Delaplace, C. Turchiuli, Prediction of droplets characteristic diameters and polydispersity index induced by a bifluid spraying nozzle by the means of dimensional analysis, Chemical Engineering Science. 265 (2023) 118187. https://doi.org/10.1016/j.ces.2022.118187.
[39] R. Hassan, K. Loubiere, J. Legrand, G. Delaplace, A consistent dimensional analysis of gas-liquid mass transfer in an aerated stirred tank containing purely viscous fluids with shear-thinning properties, Chemical Engineering Journal. 184 (2012) 42–56. https://doi.org/10.1016/j.cej.2011.12.066.
[40] G. Delaplace, Y. Gu, M. Liu, R. Jeantet, J. Xiao, X.D. Chen, Homogenization of liquids inside a new soft elastic reactor: Revealing mixing behavior through dimensional analysis, Chemical Engineering Science. 192 (2018) 1071–1080. https://doi.org/10.1016/j.ces.2018.08.023.
[41] J.D. Sullivan, C.G. Maier, O.C. Ralston, Passage of solid particles through rotary cylindrical kilns, Govt. print. off., Washington, 1927.
[42] A. Chatterjee, A.V. Sathe, M.P. Srivastava, P.K. Mukhopadhyay, Flow of materials in rotary kilns used for sponge iron manufacture: Part I. Effect of some operational variables, Metallurgical Transactions B. 14 (1983) 375–381. https://doi.org/10.1007/BF02654356.
[43] P.S.T. Sai, G.D. Surender, A.D. Damodaran, V. Suresh, Z.G. Philip, K. Sankaran, Residence time distribution and material flow studies in a rotary kiln, Metallurgical Transactions B. 21 (1990) 1005–1011. https://doi.org/10.1007/BF02670271.
[44] I.H. Hwan, Heat transfer mechanisms in an indirectly heated rotary kiln with lifters and its role in scaling, PhD manuscript, Curtin University of Technology, 2009. https://core.ac.uk/download/pdf/195633105.pdf (accessed May 16, 2014).
[45] M. Debacq, S. Vitu, D. Ablitzer, J.-L. Houzelot, F. Patisson, Transverse motion of cohesive powders in flighted rotary kilns: Experimental study of unloading at ambient and high temperatures, Powder Technology. 245 (2013) 56–63. https://doi.org/10.1016/j.powtec.2013.04.007.
[46] A.S. Bongo Njeng, S. Vitu, M. Clausse, J.-L. Dirion, M. Debacq, Residence Time Distribution - kiln 1 - sand, Recherche Data Gouv (2023). https://doi.org/10.57745/RF63PI.
[47] A.S. Bongo Njeng, S. Vitu, M. Clausse, J.-L. Dirion, M. Debacq, Residence Time Distribution - kiln 1 - broken rice, Recherche Data Gouv (2023). https://doi.org/10.57745/X6ZQBN.

[48] A.S. Bongo Njeng, S. Vitu, M. Clausse, J.-L. Dirion, M. Debacq, Residence Time Distribution - kiln 2 - beech chips, Recherche Data Gouv (2023). https://doi.org/10.57745/0BYMZL.
[49] S. Alhuthali, G. Delaplace, S. Macchietto, L. Bouvier, Whey protein fouling prediction in plate heat exchanger by combining dynamic modelling, dimensional analysis, and symbolic regression, Food and Bioproducts Processing. 134 (2022) 163–180. https://doi.org/10.1016/j.fbp.2022.05.009.
[50] M. Debacq, Data Management Plan "Rotary kilns and drums", HAL (2023). https://hal.science/hal-04004996.